Global NEST Journal, Vol 27, No 6, 07390

Assessment of CMIP6 models for precipitation simulation and prediction of future extreme precipitation in China

Rui Zhang[1,2]*, Bingfen Cheng[1,2], Bin Jiang[1,2], Bo Yang[1,2], Botao Wang[1,2] and Hongmin Zhou[3]*
[1]School of Emergency Technology and Management, North China Institute of Science and Technology, 065201, China
[2]Multi-scene water chain accident wisdom emergency technology innovation center of Hebei, 065201, China
[3]China Water Resources Beifang Investigation, Design and Research Co. Ltd. (BIDR), 300222, Tianjin
Received: 20/02/2025, Accepted: 12/04/2025, Available online: 29/04/2025
*to whom all correspondence should be addressed: e-mail: rzhang1808@163.com
https://doi.org/10.30955/gnj.07390

Graphical abstract

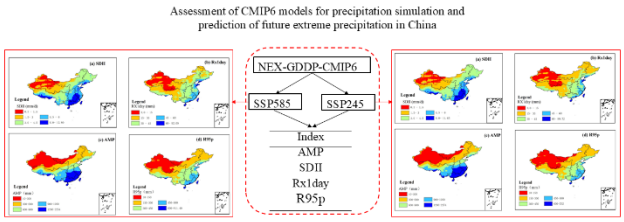

Abstract

This article evaluates the performance of 20 models from the Coupled Model Intercomparison Project phase 6 (CMIP6) in simulating precipitation over China from 1981 to 2014, with a focus on interannual and seasonal variations. The evaluations results varying levels of performance among the models, with CNRM-CM6-1 identified as the best model for simulating summer extreme precipitation. Based on CNRM-CM6-1, future projections of extreme precipitation in China have been conducted. The results indicate that under the SSP245 scenario, maximum rainfall is projected to increase primarily in southern China and southeastern Tibet. Across all extreme indices, a distinct spatial pattern emerges, characterized by a "Southeastern High – Northwestern Low" distribution throughout the study period. Under the SSP585 scenario, the spatial distribution of extreme indices mirrors that of the SSP245 scenario. However, in the late 21st century, peak values of extreme rainfall indices under the SSP585 scenario are significantly higher than those observed under the SSP245 scenario. For total precipitation, the differences between the SSP585 and SSP245 scenarios are not significant prior to 2070. However, for other indices (SDII, RX1day, R95p), the differences between the two scenarios remain minimal before 2050. After 2050, extreme precipitation indices under the SSP585 scenario become significantly higher than those under the SSP245 scenario.

Keywords: Extreme precipitation; future projections; the coupling model intercomparison program in phase 6 (CMIP6); simulation performance

1. Introduction

Studies have unequivocally demonstrated the profound negative impact of extreme climate events on both the economy and people's livelihoods. With the continued progression of global warming, extreme precipitation events are increasingly intensifying. This escalation manifests in a range of catastrophic consequences, including floods, landslides, and soil erosion, which impose a significant burden on society, the environment, and ultimately, human life safety (Wang *et al*., 2020; Nicholson *et al*., 2017; Croitoru *et al*., 2016; Brown and Funk, 2008; You *et al*., 2013; Arun Mozhi *et al*., 2024; Jasmine *et al*., 2025; Nirmal *et al*., 2025). The intensity shift of regional extreme precipitation shows an almost linear correlation with the scale of global warming. In essence, the projected magnitude of future global warming correlates with a more pronounced increase in precipitation intensity (Qiu *et al*., 2022).

The intensification of extreme rainfall stands as one of the anticipated impacts of a warming climate (Douville *et al*., 2021; AghaKouchak *et al*., 2020) for the increase in global extreme precipitation events, there is approximately a 7% increase for every 1 Kelvin rise (IPCC, 2021; Li *et al*., 2021; Wehner, 2020; Wang *et al*., 2022; Babu *et al*., 2025; Suresh *et al*., 2025). The majority of variations show increasing trends, accompanied by marked regional heterogeneity (Yuan *et al*., 2017). Xiang *et al*. (2021) estimated extreme precipitation in China based on CMIP6 data and projected a significant increase in regional extremes from 2021 to 2100. However, their analysis was based on only 14 models, with projections derived from a single selected model. Therefore, further comprehensive and robust investigations are warranted to refine and expand upon these findings.

Global Climate Models (GCMs), as crucial tools for predicting extreme climate events, have garnered increasing attention from researchers in recent years (Zhu

et al., 2020; Akinsanola *et al*., 2021). Although extreme precipitation events are projected to intensify under global warming, substantial uncertainties remain in GCM-based projections, particularly regarding simulation of regional and extreme precipitation (Eyring *et al*., 2016).

In China, CMIP5 models have been shown to reasonably capture the climatological mean state and trends of extreme precipitation to some extent (Chen and Sun, 2015). Furthermore, projections suggest that the rate of increase in extreme precipitation may surpass the global average (Sillmann *et al*., 2013). Across Asia, extreme heavy precipitation is projected to increase by at least 100% under 1.5°C and 2°C global warming scenarios (Xu *et al*., 2017). However, CMIP5 models exhibit notable limitations in simulating extreme precipitation. For example, while most models can capture the temporal trends of extreme precipitation events (Ou *et al*., 2013), significant biases are evident in their simulations of total and extreme precipitation over western China (Jiang *et al*., 2015), particularly in regions with relatively low precipitation levels. Moreover, existing studies have indicated that while the CMIP5 models provide valuable reference for predicting the frequency and intensity of future extreme precipitation events, their regional details and simulation accuracy remain limited (Zhou *et al*., 2014, 2019; Li *et al*., 2016; Wang *et al*., 2017, 2019; Peng *et al*., 2018; Xu *et al*., 2018; Karthik *et al*.,2025). These limitations underscore the need for continued advancements in climate model development.

In response to these challenges, CMIP6, as the latest update from the CMIP organization, represents a significant step forward by offering new opportunities for estimating climate variables. CMIP6 features enhanced spatial resolution and a more refined parameterization of key physical processes, addressing some of the deficiencies observed in CMIP5 (Eyring *et al*., 2016). A key improvement in CMIP6 is the incorporation of the Shared Socioeconomic Pathways (SSPs), which provide a more comprehensive framework for exploring future climate scenarios. Among these, SSP585 represents a high greenhouse gas emission scenario, characterized by rapid economic growth and limited climate change mitigation efforts, while SSP245 reflects an intermediate emission scenario with moderate mitigation actions and a focus on sustainability. These scenarios allow for a more detailed and systematic examination of future climate conditions and their potential impacts. Evaluating the ability of GCMs under CMIP6 to replicate historical precipitation events can provide valuable insights into improving future climate forecasts (Prein *et al*., 2017; Bai *et al*., 2007; Chen *et al*., 2012).

CMIP6 models have shown significant improvements in spatial resolution and physics, including a refined parametrization of aerosol effects (Eyring *et al*., 2016; Gusain *et al*., 2020). The results from CMIP6 models incorporate more complex and revised parametric approaches for dynamical processes, and introduce a new emission scenario for projections (O'Neill *et al*., 2014; Gusain *et al*., 2020). Hence, enhancing the capability of CMIP6 models to simulate extreme rainfall remains critical, as this represents a major source of uncertainty in climate change projections (Kawai *et al*., 2019; Park *et al*., 2019). Recent efforts to evaluate and predict climatic extremes have been conducted using CMIP6 models (Jiang *et al*., 2020; Chen *et al*., 2020b). Chen *et al*. (2020b) reported that the CMIP6 multi-model median ensemble (MME) demonstrated overall improvements in simulating global climatic means and extremes compared to CMIP5, with reduced model uncertainties. In China, it is anticipated that both temperature and rainfall will increase by the end of the twenty-first century, with the most significant increases in annual precipitation expected in northern and western regions (Yang *et al*., 2021). Numerous global studies have shown an overall improvement in the ability of climate models to simulate extreme rainfall. However, in regions with complex topography such as the Qinghai-Tibet Plateau, the improvement over CMIP5 models remains limited (Lun *et al*., 2021). However, these studies have mainly focused on the performance of annual average precipitation or a single extreme precipitation index of the CMIP6 model, with few systematic studies conducted on their overall performance.

This study evaluates the performance of 20 GCMs models from CMIP6 in simulating regional precipitation across China and investigates the spatiotemporal variations of extreme precipitation indices under SSP245 and SSP585 scenarios. The main objectives are to identify the most suitable model for simulating summer precipitation and to characterize future changes in extreme precipitation across different periods. By systematically assessing model performance, the study offers critical insights into model selection for future climate applications. The results have important implications for the sustainable management and planning of water resources in China under changing climate conditions.

2. Data and methods

2.1. Data

This study used the CN05.1 grid dataset, which is interpolated from observational data recorded at over 2400 ground-based meteorological stations in China. The dataset used in this study was provided by the Climate Change Research Center, Chinese Academy of Sciences (https://ccrc.iap.ac.cn/resource/detail?id=228). It was subjected to strict quality control and homogenization checks before release. This dataset, which is used widely in precipitation research in China, has spatial resolution of 0.25° (approximately 25 km × 25 km). The historical data for the years 1981–2014 were used in this study.

The first version of the NASA Earth Exchange Global Daily Downscaled Projections (NEX-GDDP) dataset, NEX-GDDP-CMIP5, was released in 2015 and has been widely applied in studies of climate change impacts at both global and local scales (Kumar *et al*. 2020; Zhang *et al*., 2019; Zeng *et al*., 2019). The latest version, NEX-GDDP-CMIP6, includes downscaled data from 35 models spanning 1950 to 2100 (covering both historical and future periods) based on

CMIP6 model outputs (Thrasher *et al*., 2022; Zhang *et al*., 2024). The bias correction and spatial disaggregation (BCSD) method was applied to the NEX-GDDP-CMIP6 dataset to uniformly downscale the original CMIP6 output to daily data with a spatial resolution of 0.25°. The NEX-GDDP-CMIP6 dataset was calibrated using a global meteorological forcing dataset, which incorporated both reanalysis data and observations (Sheffield *et al*., 2006; Thrasher *et al*., 2022).

Considering the consistency of scenarios and time periods, we selected 20 downscaled model simulations (**Table 1**) with daily precipitation data spanning 2025–2100 under two SSP-RCP scenarios (SSP245 and SSP585) across China to predict future extreme precipitation indices. Detailed information and documentation on the NEX-GDDP-CMIP6 dataset are available online at https://www.nccs.nasa.gov/services/data-collections/land-based-products/nex-gddp-cmip6.

Table 1 Basic Information on 20 CMIP6 Global Climate Models

No.	Names	Country (region)	CMIP6 mode original resolution (Longitude × Latitude)	NEX-GDDP resolution (Longitude × Latitude)
1	ACCESS-CM2	Australia	1.9° × 1.3°	0.25°× 0.25°
2	ACCESS-ESM1-5	Australia	1.9° × 1.2°	0.25° × 0.25°
3	CanESM5	Canada	2.8° × 2.8°	0.25° × 0.25°
4	CMCC-CM2-SR5	Italy	1.3° × 0.9°	0.25° × 0.25°
5	CMCC-ESM2	Italy	1.3° × 0.9°	0.25° × 0.25°
6	CNRM-CM6-1	France	1.4° × 1.4°	0.25° × 0.25°
7	CNRM-ESM2-1	France	1.4° × 1.4°	0.25° × 0.25°
8	EC-Earth3	European Union	0.7° × 0.7°	0.25° × 0.25°
9	EC-Earth3-Veg-LR	European Union	1.1°× 1.1°	0.25° × 0.25°
10	FGOALS-g3	China	2.0° × 2.3°	0.25° × 0.25°
11	GFDL-CM4(gr1)	America	1.0° × 1.0°	0.25° × 0.25°
12	GFDL-CM4(gr2)	America	1.0° × 1.0°	0.25° × 0.25°
13	GFDL-ESM4	America	1.0° × 1.0°	0.25° × 0.25°
14	GISS-E2-1-G	America	2.5° × 2.0°	0.25° × 0.25°
15	INM-CM4-8	Russia	2.0° × 1.5°	0.25° × 0.25°
16	INM-CM5-0	Russia	2.0° × 1.5°	0.25° × 0.25°
17	IPSL-CM6A-LR	France	2.5° × 1.3°	0.25° × 0.25°
18	MIROC6	Japan	1.4° × 1.4°	0.25° × 0.25°
19	MIROC-ES2L	Japan	2.8° × 2.8°	0.25° × 0.25°
20	MPI-ESM1-2-HR	Germany	0.9° × 0.9°	0.25° × 0.25°

This high-quality downscaled dataset is well-suited for evaluating the impacts of climate change on processes sensitive to small-scale climate gradients and topographic influences. It enables detailed analyses of climate characteristics at the watershed scale.

2.2. Methods

Accurate observational precipitation data are crucial for evaluating the precipitation simulation capabilities of selected models. This study used daily precipitation data from the CN05.1 dataset as reference to evaluate the ability of 20 models to simulate the NEX-GDDP precipitation patterns from 1981 to 2014. All calculations were performed using MATLAB R2023a and ArcGIS 10.8.

2.2.1. Evaluation and analysis methods

The calculation formula for the correlation coefficient (*CC*) is given by Equation 1 (Dong *et al*., 2015):

$$CC=\frac{\sum_{i=1}^{n}\left[(Y_{i,obs}-\overline{Y_{obs}})(Y_{i,sat}-\overline{Y_{sat}})\right]}{\sqrt{\left[\sum_{i=1}^{n}(Y_{i,obs}-\overline{Y_{obs}})^2\right]}\sqrt{\left[\sum_{i=1}^{n}(Y_{i,sat}-\overline{Y_{sat}})^2\right]}} \quad (1)$$

The standard deviation (*SD*) calculation formula is given by Equation 2:

$$SD=\sqrt{\frac{\sum_{i=1}^{n}(X_i-\bar{X})}{N-1}} \quad (2)$$

The formula for calculating the root mean square error (*RMSE*) is given by Equation 3:

$$RMSE=\sqrt{\frac{\sum_{i=1}^{n}(Y_{i,obs}-Y_{i,sat})^2}{n}} \quad (3)$$

In Equations (1)–(3), $Y_{i,\,obs}$ represents the observed rainfall data of the *i*-th station; $Y_{i,\,sat}$ represents the pattern rainfall data of the *i*-th station, $\overline{Y_{obs}}$ represents the average observed rainfall at the station; $\overline{Y_{sat}}$ represents the average models rainfall of the station; X_i represents the statistical values of each station; $\bar{X}$ is the average value of indices for each station; *N* is the number of stations.

2.2.2. Extreme precipitation indices (EPIs)

The Expert Group on Climate Change Monitoring and Extreme Climate Event Indicators (ETCCDI) of the World Meteorological Organization proposed a set of extreme climate event indices at the Climate Change Monitoring Conference from 1998 to 2001, which subsequently formed unified guidelines in the field of climate change

research. The fourth report of the IPCC redefined extreme climate, with 27 indices identified as core indices (Croitoru *et al.*, 2016). However, there is a strong correlation between different indices. This article selects four indices, which represent total rainfall (annual average rainfall), rainfall intensity (total rainfall/rainfall days), maximum daily rainfall (maximum daily rainfall per year), extreme rainfall (total rainfall with daily rainfall exceeding 95% threshold per year) are shown in **Table 2**.

Based on the selected extreme indices, we analyzed the changes in extreme indices from 2025 to 2100 under different scenarios.

Table 2 Extreme Precipitation Index (Wet days are defined as days with precipitation>1 mm)

Index	Definition	Unit
AMP	annual average rainfall	mm
SDII	total rainfall/rainfall days	mm/day
Rx1day	maximum daily rainfall per year	mm
R95p	total daily rainfall exceeding 95% threshold per year	mm

3. Results and discussions

3.1. Evaluation of simulation ability of models

3.1.1. Evaluation of simulation capability for spatial climate state characteristics

To assess the capability of simulating average annual precipitation in China using downscaled data from NEX-GDDP-CMIP6, this study calculated the averages of observed data, model outputs, and their differences (**Figure 1**). Based on the observations and multi-model ensemble (MME) mean, the results reveal significant spatial heterogeneity in multi-year average precipitation across China, decreasing from over 1600 mm in the southeast to less than 200 mm in the northwest (**Figure 1a, b**). The MME mean more effectively reproduces the spatial distribution characteristics of observed annual mean precipitation. As shown by the difference between observations and the MME mean (**Figure 1c**), the MME tends to underestimate the average annual precipitation by more than 150 mm in most parts of China, especially in the south and northwest. Notably, in Tibet, the MME mean significantly overestimates the precipitation, with differences exceeding 150 mm.

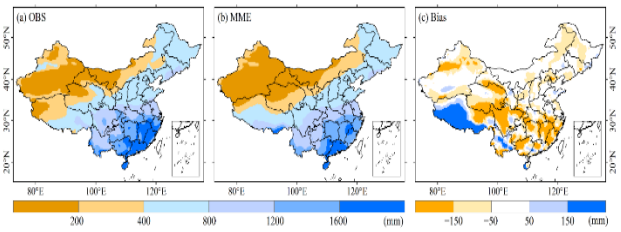

Figure 1. The CMIP6 model downscale data simulates the spatial characteristics of the annual average precipitation from 1981 to 2014. (a) is the observed value, (b) is the MME mean, and (c) is the difference field between the MME mean and the observed values. There is no observed data in Taiwan, China, which is not included in the statistics

3.1.2. Evaluation of simulation capability for spatial climate state characteristics of seasonal precipitation

This study further assessed the ability of CMIP6 model downscaled data to reproduce the spatial patterns of seasonal precipitation in China (**Figure 2**). Based on observations, the spatial distribution of average spring precipitation in China exhibits a gradient, with higher values in the southeast and lower values in the northwest (**Figure 2a**). In the southeast, average spring precipitation exceed 500 mm, while in the northwest it is less than 20 mm. The MME mean for spring generally captures this distribution, though the region with very low precipitation (<10 mm) in the northwest is larger than observed (**Figure 2b**). The difference between the MME mean and observations indicates relatively small discrepancies in the northern China, with an error range of approximately ±25 mm. Most areas in the south show moderate differences (around 50 mm), while anomalies of around 50 mm are more prevalent in the hinterland and southern parts of the Qinghai-Tibet Plateau. In summer, observed national average precipitation is higher than in other seasons, with maximum values exceeding 500 mm in southern and southeastern China, and minimum values below 50 mm in the northwest (**Figure 2d**). The MME mean replicates the overall spatial pattern, but underestimation in the northwest is more pronounced, particularly in south western Xinjiang, where the average annual precipitation is below 10 mm. (**Figure 2e**). The difference between the MME mean and the observation (**Figure 2f**) indicates that the MME mean is underestimated in most regions of the country, but clearly overestimated in the Qinghai-Tibet Plateau.

In autumn, both the observational data and MME mean depict a spatial distribution pattern with high precipitation levels in the southeast and low levels in the northwest. The high values are concentrated in the southeast, exceeding 200 mm, while the low values are predominantly found in the northwest, with less than 20 mm of precipitation (**Figure 2g, h**). The variation in average precipitation during autumn suggests that the error in the MME mean for this season is relatively low. Specifically, there is a relatively minor deviation observed in central China, eastern China, and northern Xinjiang. However, there is a slight overestimation, exceeding 25 mm, in the southern part of the Qinghai-Tibet Plateau. Notably, the overestimation in Sichuan province is less pronounced compared to that in spring and summer (**Figure 2i**).

In winter, the results show that except for the southeastern region where precipitation averages higher (100-500 mm), most regions across the country

experience lower precipitation levels (<50 mm). The MME mean reflects a similar spatial distribution as observed. However, the phenomenon of reduced precipitation in the northern areas is more extensive, with levels dropping below 10 mm (**Figure 2j, k**). The discrepancy in average winter precipitation suggests that the MME mean slightly underestimates precipitation in the southeastern part of China, while it slightly overestimates (with an approximate 25-50 mm underestimation) precipitation along the western edge of China (**Figure 2l**).

Overall, MME mean effectively captures the spatial variability of seasonal annual precipitation across China. However, it tends to overestimate precipitation in the Qinghai-Tibet Plateau, while underestimating it in most other regions.

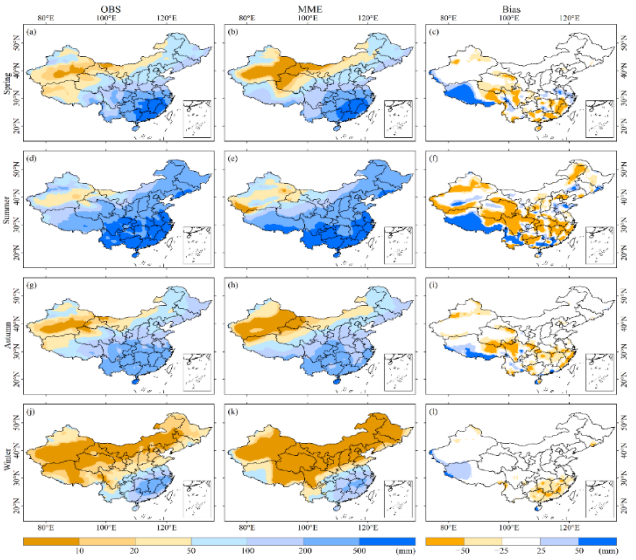

Figure 2. The CMIP6 model downscale data simulates the spatial characteristics of precipitation in different seasons from 1981 to 2014. The first to fourth rows represent spring, summer, autumn, and winter, with the leftmost column representing the observed values, the middle column representing MME mean, and the rightmost column representing the difference between the MME mean and the observed values

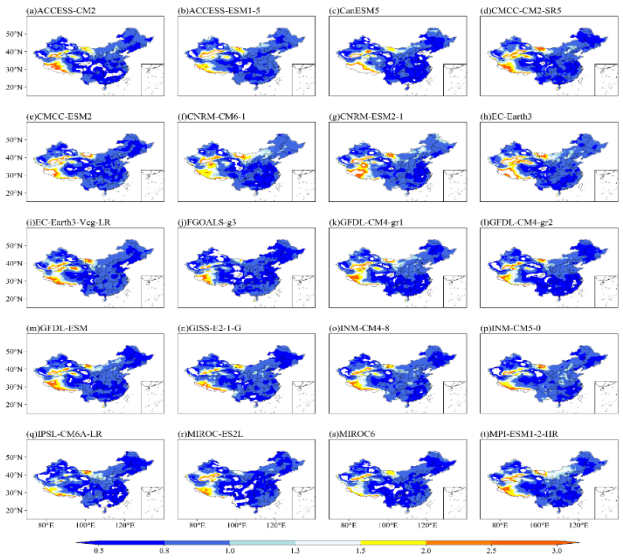

Figure 3. Ratio of standard deviation of downscale annual precipitation to standard deviation of observed values for each CMIP6 model from 1981 to 2014

3.1.3. Spatial evaluation indices for precipitation

This study further investigated the SD ratio, and RMSE at each model grid point compared to observations (**Figure 3 and Figure 4**).

The standard deviation ratio is notably higher in the southwest (>2), indicating relatively larger amplitude in this region. Although the simulated amplitudes in most regions are close to the observed values, they are generally lower, likely due to smoothing of the model values (**Figure 3**). **Figure 4** illustrates that each model demonstrates lower root mean square error in northern China but higher error in the southern region, suggesting a higher error in the south compared to the north.

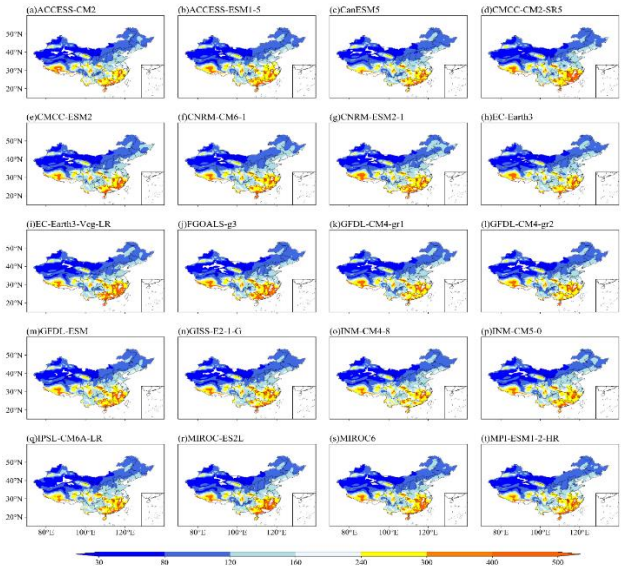

Figure 4. RMSE between the SD of downscale annual precipitation and observed values for each CMIP6 model from 1981 to 2014 (unit: mm)

In order to further evaluate the spatial characteristics of the average annual precipitation of various models in China, this study used Taylor plots to evaluate the spatial characteristics of the total annual precipitation.

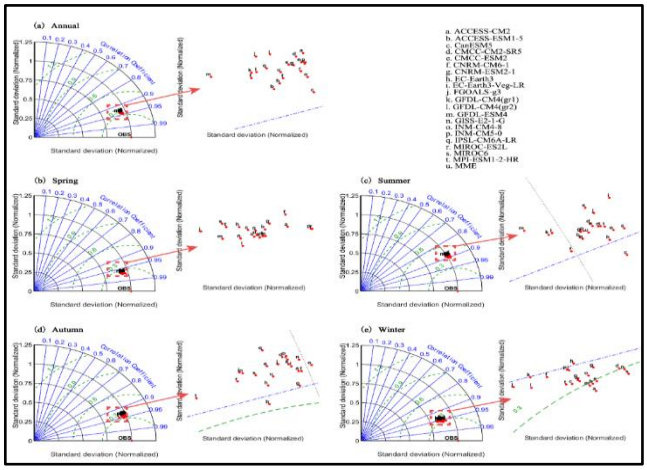

Figure 5. Taylor plot of the average annual precipitation simulated by the downscaling models of the CMIP6 model. The radian scale is CC, y-axis is the ratio of the standard deviation (STD) between the simulated and observed values, the green semicircle represents RMSE, (a) year, (b) spring precipitation, (c) summer precipitation, (d) autumn precipitation, and (e) winter precipitation

According to **Figure 5a**, at the annual scale, the spatial correlation coefficient (R) between all model grid points and observation grid points in the 20 models ranges between 0.9 and 0.95. This suggests that the simulated annual precipitation from each model exhibits a high correlation coefficient with observed values regarding spatial climate patterns. The standardized standard deviation of the total annual precipitation simulated by all models is approximately 0.9, indicating that the spatial distribution differences of the model simulation values are slightly smaller than the observed values, implying slightly smaller spatial fluctuation amplitudes. The central root mean square error of the simulated annual average precipitation for each model is around 0.4, indicating a small error. The differences in the three indicators among each model in the Taylor plot are relatively small, suggesting that the MME mean yields a better simulation effect on the climate state of the annual average precipitation in China.

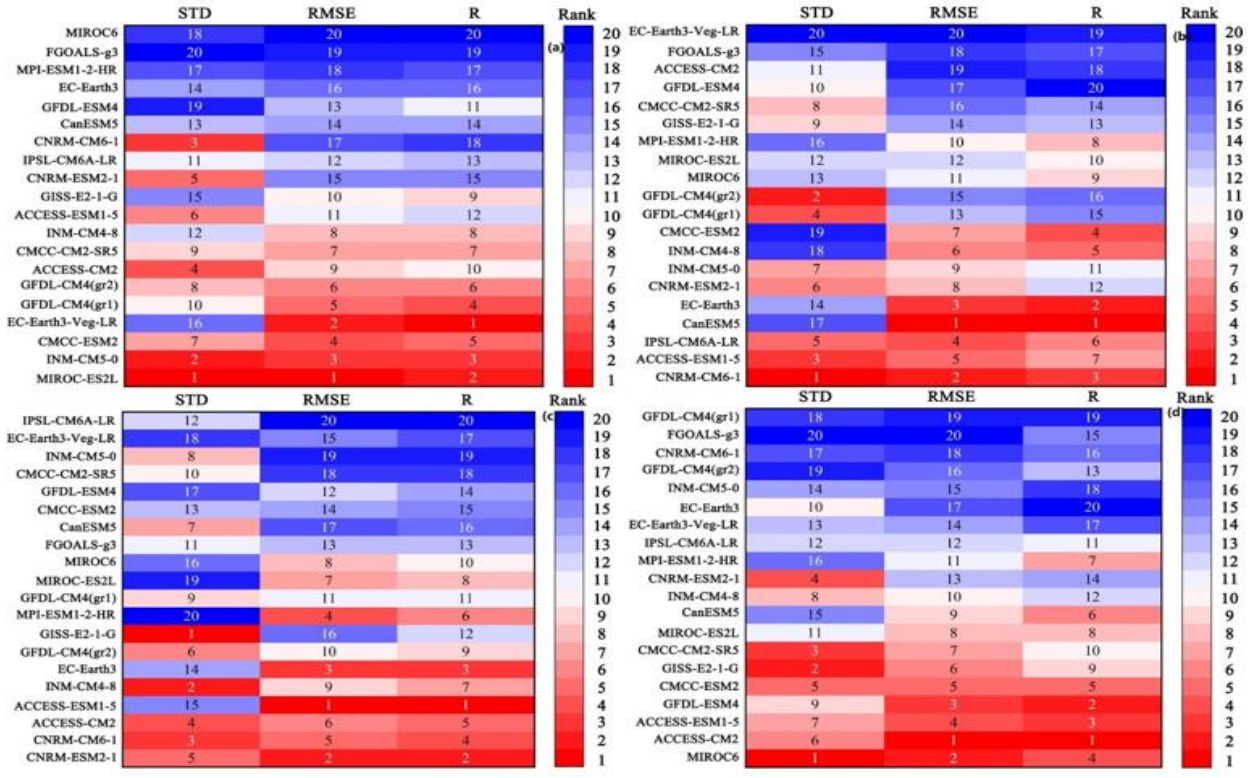

Figure 6. The spatial performance of different seasonal patterns was sorted (a) Spring Precipitation, (b) Summer Precipitation, (c) Autumn Precipitation, (d) Winter Precipitation

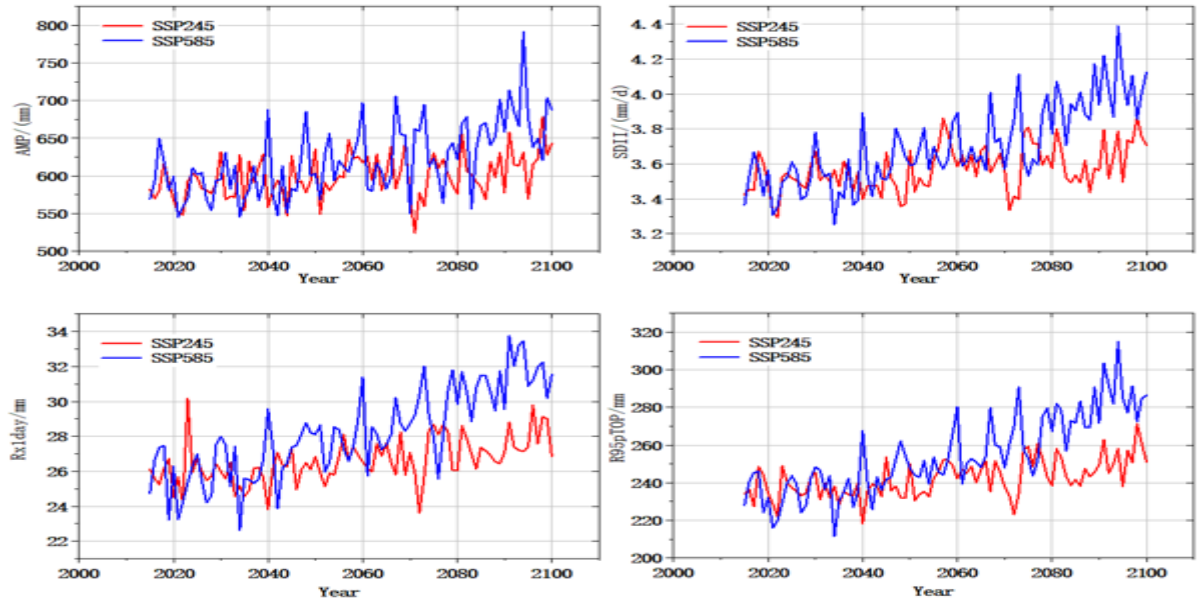

Figure 7. Annual mean change trend of extreme indices under two scenarios

According to **Figures 5b-e**, across seasons, the spatial *CC* between all model grid points and observation grid points in the 20 models exceeds 0.9, except for summer where it falls slightly below 0.9. This suggests a high correlation between the total simulated seasonal precipitation in each model and observed values in terms of spatial climate patterns. The *STD* of total seasonal precipitation simulated by all models is slightly below 1, indicating that spatial distribution differences in model simulation values are slightly smaller than observed values, implying a slightly reduced spatial fluctuation amplitude. The *RMSE* of each model in simulating seasonal precipitation is approximately 0.4, indicating minimal error. Variations in these indicators among models in the Taylor plot are relatively small, indicating a favorable average simulation effect of each model and model set on the seasonal total precipitation climate state in China. Based on the *CC*, *STD*, and *RMSE* values in the Taylor plot, and employing the CRI ranking method, this study ranked the spatial performance of different seasonal patterns, as depicted in **Figure 6**. The top five patterns in spring spatial performance rankings are MIROC-ES2L, INM-CM5-0, CMCC-ESM2, EC-Earth3-Veg-LR, and GFDL-CM4 (gr1). The top five modes in summer rankings are CNRM-CM6-1, ACCESS-ESM1-5, IPSL-CM6A-LR, CanESM5, and EC-Earth3.The top five modes in autumn rankings are CNRM-ESM2-1, CNRM-CM6-1, ACCESS-CM2, ACCESS-ESM1-5, and INM-CM4-8.The top five modes in winter rankings are MIROC, ACCESS-CM2, ACCESS-ESM1-5, GFDL-ESM4, and CMCC-ESM2.Overall, for different seasons, even for the same precipitation indicator (total precipitation), the ranking of the patterns varies. Since extreme precipitation in China primarily occurs during summer, the analysis of future extreme precipitation is based on the highest-ranked model for the summer season, CNRM-CM6-1. Projections were conducted under two scenarios.

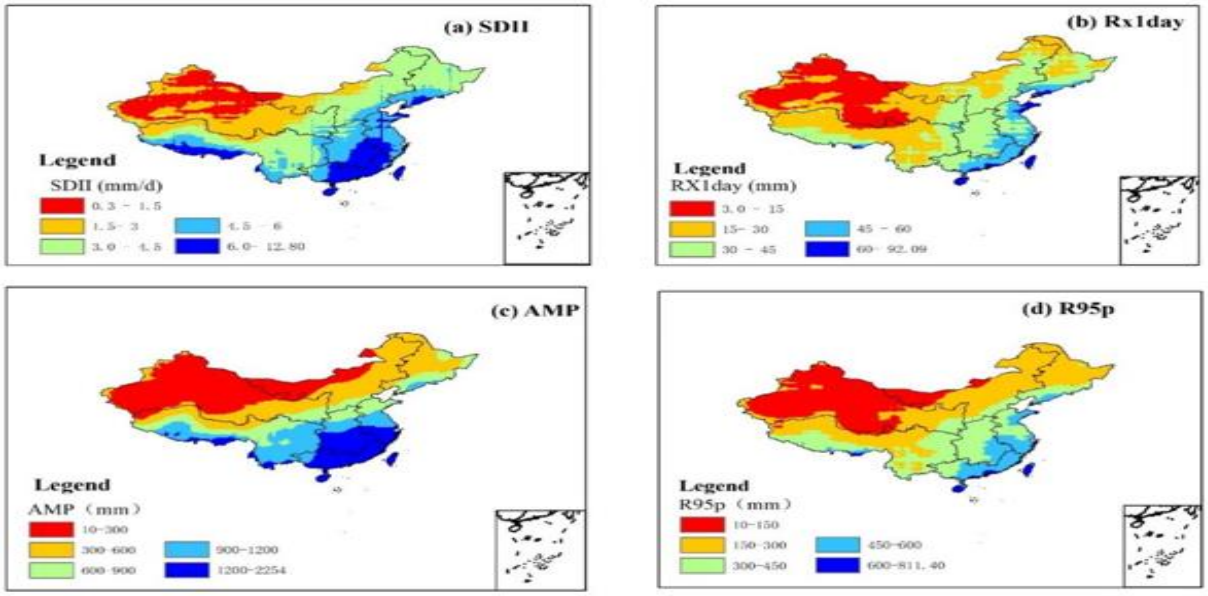

Figure 8. Spatial changes of extreme precipitation indices under SSP585

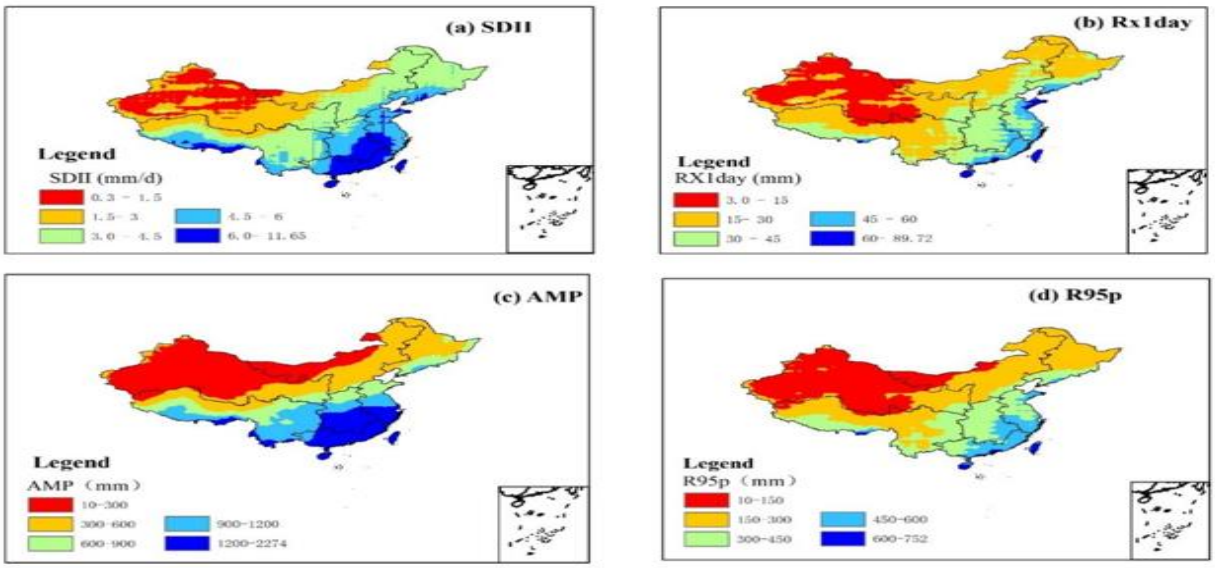

Figure 9. Spatial changes of extreme precipitation indices under SSP245

3.2. Analysis of EPIs in future

3.2.1. Changes in extreme precipitation indices under two scenarios

Figure 7 presents the annual average values of each extreme indicator over time under the SSP245 and SSP585 scenarios. It's worth noting that, in the early 21st century, there was negligible disparity in SDII between the two scenarios. However, as time progressed, although both scenarios exhibited an increasing trend, the SDII value under the SSP585 scenario surpassed that under the SSP245 scenario, reaching a maximum annual average of 4.39 mm/day. The Rx1day trend closely mirrors that of SDII, with its peak value reaching 33.75 mm in the late 21st century. R95pTOP demonstrates similar changing characteristics, and by the late 21st century, there was a notable disparity in the annual mean of R95pTOP between the two scenarios. Under the SSP585 scenario, the highest value reached 314.77 mm, approximately 40 mm higher than under the SSP245 scenario.

In the near and mid-21st century, there was no discernible difference in AMP between the two scenarios. However, by the end of the century, the AMP value under the SSP585 scenario gradually exceeded that under the SSP245 scenario. The highest AMP value under the SSP585 scenario reached 791 mm, about 82 mm higher than that under the SSP245 scenario.

Based on the temporal variation patterns of various extreme indicators, it becomes apparent that in the future, extreme precipitation will exhibit a more pronounced upward trend in response to scenario changes, indicating an overall increase in extreme precipitation. The recent increase in the 21st century has been relatively gradual, with minimal discrepancies between scenarios. However, the rate of increase from the mid to late 21st century has progressively accelerated, leading to more noticeable differences between scenarios.

3.2.2. Spatial changes in extreme precipitation indices under two scenarios

Emission scenarios have a significant impact on both the magnitude and spatial distribution of extreme precipitation. **Figure 8** shows the spatial distribution of extreme precipitation indices under the SSP585 scenario. Under this scenario, the spatial distribution of extreme precipitation indices exhibits a gradual increase, increasing from northwest to southeast.

The SDII is higher in southeastern Tibet, as well as in Hainan, Guangdong, and Jiangxi provinces, indicating that under high-emission scenarios, these regions are expected to experience higher rainfall intensities, with a maximum value of up to 12.8 mm/day. The spatial distribution trend of the maximum one-day precipitation (R1xday) is similar to that of SDII. Regions with values between 15 mm and 45 mm cover a broader area compared to other precipitation intensity ranges, with the highest values primarily located in Hainan and coastal Guangdong.

The AMP (annual maximum precipitation) also reaches its highest values in the southeastern coastal regions of China, peaking at 2254 mm. The distribution of R95p (precipitation on very wet days) closely resembles that of R1xday, with areas exceeding 300 mm accounting for nearly half of the total area.

Figure 9 shows the spatial distribution of extreme precipitation indices under the SSP245 scenario. The spatial distribution is similar to that under the SSP585 scenario, both exhibiting a stepped pattern with an increasing trend from northwest to southeast. The highest SDII value is slightly lower than that under the SSP585 scenario, at 11.65 mm/day. The distribution trend of the Rx1day is similar to that of SDII, with the 15–45 mm range covering a broader area compared to other precipitation values, and the highest value is also lower than that under the SSP585 scenario. The distribution area of AMP is almost identical to that under the SSP585 scenario, but the highest value is slightly higher. The distribution area of R95p is nearly the same as under the SSP585 scenario, but its highest value is slightly lower.

Based on the above analysis, R95p and SDII have shown significant increases in East and South China, indicating a trend toward more concentrated precipitation in these regions. Notably, Southwest and Central China have also experienced substantial rises in extreme precipitation indices, suggesting an elevated risk of heavy rainfall events in the future. Although increase in extreme precipitation intensity are also observed in Northwest, Northeast, and North China, the magnitude of change in these areas is comparatively lower. These findings are consistent with previous studies (Zhu *et al*., 2021; Xu *et al*., 2022), further underscoring the regional variations in precipitation trends and their potential implications for future climate scenarios.

Compared with previous research, this provides a more comprehensive assessment of projected shifts in extreme precipitation across different regions of China. It considers the distinct response patterns of extreme precipitation to climate warming under two socio-economic scenarios. Our analysis highlights the similar trends in extreme precipitation changes across Central and Southwest China. Furthermore, we observe a discernible escalation in the rate of extreme precipitation intensity across Northwest, North, and Northeast China, accompanied by a significant elevation in R50. Importantly, the precipitation dynamics observed in East and South China depict a more focused trend, characterized by a substantial surge in R50 and similar change rates.

Improving pattern performance involves more than enhancing model resolution. When resolution upgrades do not significantly improve overall model performance, pattern performance remains unchanged (Wang *et al*., 2014). This observation helps elucidate why CMIP6's capacity to simulate average extreme precipitation significantly improves in arid and semi-arid regions following resolution enhancements, whereas the improvements are less pronounced in humid regions. Additionally, addressing the reduction of uncertainty between models stands as a pivotal focus for refining the accuracy of long-term precipitation climate predictions,

necessitating further in-depth investigation (Zhou *et al*., 2020).

4. Conclusions

The primary objective of this study was to evaluate the performance of CMIP6 models in simulating precipitation patterns across China. The analysis results indicate a clear trend of increasing extreme precipitation events throughout the country, consistent with findings from Seneviratne *et al*. (2012), who projected that climate change would lead to an increase in the frequency and intensity of extreme weather events on a global scale. For this assessment, data from 20 models were selected and analyzed based on availability, ensuring a comprehensive evaluation of precipitation trends. The results show that several models exhibit satisfactory performance, with future projections of extreme precipitation indices revealing varying trends. The key findings of this study can be summarized as follows:

(1) The study projects a clear upward trend in extreme precipitation events under both future climate scenarios, with significant regional variations. The spatial distribution of inter-annual precipitation deviations across China, as simulated by various models, reveals a consistent underestimation in the central and southeastern regions (approximately 150 mm lower), while the hinterland and southern regions of the Qinghai-Tibet Plateau show a significant overestimation (approximately 150 mm higher). These discrepancies are likely influenced by the high altitudes and complex terrain of the plateau, which may limit the model's ability to accurately simulate precipitation in these regions.

(2) The models generally perform well in simulating the spatial distribution of average annual precipitation across China, with errors generally within 10%. Among the various models, CNRM-CM6-1 demonstrated the best performance in simulating summer precipitation, according to seasonal evaluation results.

(3) Under the SSP245 scenario, extreme precipitation is projected to increase significantly, particularly in southeastern China and southeastern Tibet. The spatial pattern follows a southeast-to-northwest gradient, with the highest CWD reaching 53.5 days in the southwest by the late 21st century, while remaining below one day in the northwest. Under SSP585, these trends are further intensified, indicating a more severe future hydrological regime. These findings underscore the importance of implementing region-specific climate adaptation strategies.

This study provides valuable insights into future extreme precipitation patterns across China but is limited by challenges in accurately simulating regions with complex topography, such as the Qinghai‑Tibet Plateau. Model biases in high-altitude areas underscore the need for higher spatial resolution and improved representation of orographic effects. While consistent with previous projections (Xu *et al*., 2017; Jiang *et al*., 2021), our findings offer enhanced regional granularity and reveal marked spatial heterogeneity, particularly in southeastern and plateau regions. Future efforts should focus on refining model performance in complex terrains and employing high-resolution downscaling to support localized climate risk assessments.

Acknowledgements

This work was supported by the "Langfang Science and Technology Support Plan Project" (No. 2024013033, 2024013020, 2023013101), "Science Research Project of Hebei Education Department" (No QN2025850), "Fundamental Research Funds for the Central Universities" (No.3142023019, No.3142023021, 3142023017, 3142021002), the Central Government Guides Local Funds for Science and Technology Development (No. 236Z0307G).

Data Availability Statement: The grid data used in this article comes from https://cds.nccs.nasa.gov/nex-gddp/. The observation data is from the China Meteorological Data Network (http://data.cma.cn/).

Author Contributions

Formal analysis, Rui Zhang; Funding acquisition, Rui Zhang, Bingfen Cheng, Bin Jiang, Bo Yang; Methodology, Rui Zhang, Bingfen Cheng; Supervision, Rui Zhang; Validation, Botao Wang, Bo Yang; Writing – original draft, Rui Zhang; Writing – review & editing, Hongmin Zhou. All authors have read and agreed to the published version of the manuscript.

Conflicts of interest

The authors declare no conflicts of interest.

References

AghaKouchak A., Chiang F., Huning L.S. *et al*. (2020), Climate extremes and compound hazards in a warming world, *Annual Review of Earth and Planetary Sciences*, **48,** 519–548. https://doi.org/10.1146/ANNUREV-EARTH-071719-055228.

Akinsanola A. A., Victor O., Gabriel J. K. (2021), Evaluation of CMIP6 models in simulating the statistics of extreme precipitation over Eastern Africa, *Atmospheric Research*, **254**, 105509. https://doi.org/ 10.1016/j.atmosres.2021.105509.

Arun M.S.S., Sundara R. N., Hemlathadhevi A., Surendran R. (2025). A Light weighted Dense and Tree structured simple recurrent unit (LDTSRU) for flood prediction using meteorological variables, *Global NEST Journal*. DOI: 10.30955/gnj.06242

Babu T., Raveena S., Tamilvizhi T. and Surendran R. (2024), Integrated Early Flood Prediction using Sentinel-2 Imagery with VANET-MARL-based Deep Neural RNN, *Global NEST Journal*, **26**(10). DOI: 10.30955/gnj.06554

Bai A.J., Zhai P.M., Liu X.D. (2007), Climatology and trends of wet spells in China, *Theoretical and Applied Climatology*, **88**(3–4):139–148. doi:10.1007/s00704-006-0235-710.1002/

Brown M.E. and Funk C.C. (2008), Food Security under climate Change, *Science*, **319,** 580–581. https://doi.org/10.1126/science.1154102

Chen H.P., Sun J.Q., Chen X.L. *et al*. (2012), CGCM projections of heavy rainfall events in China, *International Journal of Climatology*, **32**(3): 441-450. doi:10.1002/joc.2278.

Chen H. and Sun J. (2015), Assessing model performance of climate extremes in China: an inter-comparison between CMIP5 and CMIP3, *Climatic Change*, **129**(1–2): 197–211. doi:10.1007/s10584-014-1319-5.

Chen H., Sun J., Lin W. *et al*. (2020), Comparison of CMIP6 and CMIP5 models in simulating climate extremes, *Science Bulletin*, **65**(17), 1415–1418.

Croitoru A., Piticar A. and Burada D.C. (2015). Changes in precipitation extremes in Romania, *Quaternary International*, **415,** 325–335. doi:10.1016/ j.quaint.2015.07.028.

Dong S.Y., Xu Y., Zhou B.T. *et al*. (2015). Assessment of indices of temperature extremes simulated by multiple CMIP5 models over China, *Advances in Atmospheric Sciences*, **32**(8), 1077–1091.

Douville H., Raghavan K. and Renwick J. (2021), Water cycle changes, In: Climate Change 2021: The Physical Science Basis. Contribution of Working Group I to the Sixth Assessment Report of the Intergovernmental Panel on Climate Change. [Masson-Delmotte V., Zhai P., Pirani A., *et al*.], Cambridge University Press, Cambridge, United Kingdom and New York, NY, USA, 1055–1210. doi:10.1017/ 9781009157896.010.

Eyring V., Bony S., Meehl G.A. *et al.* (2016), Overview of the Coupled Model Intercomparison Project Phase 6 (CMIP6) experimental design and organization, *Geoscientific Model Development*, **9**(5): 1937–1958. doi:10.5194/gmd-9-1937-2016.

Gusain A., Ghosh S. and Karmakar S. (2020), Added value of CMIP6 over CMIP5 models in simulating Indian summer monsoon rainfall, *Atmospheric Research*, **232**: 104680. doi:10.1016/j.atmosres.2019.104680.

IPCC. (2021), Climate Change 2021: The Physical Science Basis. Contribution of Working Group I to the Sixth Assessment Report of the Intergovernmental Panel on Climate Change [R], Cambridge University Press, Cambridge, United Kingdom.

Li C., Zwiers F., Zhang X. *et al*. (2021), Changes in annual extremes of daily temperature and precipitation in CMIP6 models, *Journal of Climate*, **34**(9): 3441–3460. doi:10.1175/JCLI-D-19-1013.1.

Li W., Jiang Z.H., Xu J.J. *et al.* (2016), Extreme precipitation indices over China in CMIP5 models. Part II: probabilistic projection, *Journal of Climate*, **29**: 8989–9004.

Jasmine J., Sonia J. R., Ramesh T. and Surendran R. (2025), Advanced Weather Prediction based on Hybrid Deep Gated Tobler's Hiking Neural Network and robust Feature Selection for tackling Environmental Challenges, *Global NEST Journal*, **27**(4), https://doi.org/10.30955/gnj.06757.

Jiang D., Hu D., Tian Z. *et al*. (2020), Differences between CMIP6 and CMIP5 models in simulating climate over China and the East Asian monsoon, *Advances in Atmospheric Sciences*, **37**: 1102–1118.

Jiang Z.Z., Li W., Xu J.J. *et al*. (2015), Extreme precipitation indices over China in CMIP5 models. Part I: Model evaluation, *Journal of Climate*, **28**(21): 8603–8619.

Karthik S., Surendran R., Sam Kumar G.V, Senduru S. (2025), Flood Prediction in Chennai based on Extended Elman Spiking Neural Network using a Robust Chaotic Artificial Hummingbird optimizer, *Global NEST Journal*, DOI: 10.30955/gnj.07113

Kawai H., Yukimoto S., Koshiro T. *et al*. (2019), Significant improvement of cloud representation in the global climate model MRI-ESM2, *Geoscientific Model Development*, **12**: 2875–2897.

Kumar P., Kumar S., Barat A. *et al*. (2020), Evaluation of NASA's NEX-GDDP-simulated summer monsoon rainfall over homogeneous monsoon regions of India, *Theoretical and Applied Climatology*, **141**: 525–536.

Lun Y., Liu L., Cheng L. *et al*. (2021), Assessment of GCMs simulation performance for precipitation and temperature from CMIP5 to CMIP6 over the Tibetan Plateau, *International Journal of Climatology*, **41**(7): 3994–4018.

Nicholson S.E. (2017), Climate and climatic variability of rainfall over eastern Africa, *Reviews of Geophysics*, **55**(3), 590–635.

Nirmal Kumar M., Subramanian P. and Surendran R. (2025), Multivariate time series weather forecasting model using integrated secondary decomposition and Self-Attentive spatiotemporal learning network, *Global NEST Journal*, **27**(4). DOI: 10.30955/gnj.06195

Ou T.H., Chen D.L., Linderholm H.W. *et al*. (2013), Evaluation of global climate models in simulating extreme precipitation in China, *Tellus A*, **65**: 19799.

O'Neill B.C., Kriegler E., Riahi K. *et al*. (2014), A new scenario framework for climate change research: the concept of shared socioeconomic pathways, *Climatic Change*, **122,** 387–400.

Park S.S., Shin J.H., Kim S.Y. *et al*. (2019), Global climate simulated by the Seoul National University Atmosphere Model Version 0 with a Unified Convection Scheme (SAM0-UNICON), *Journal of Climate*, **32**: 2917–2949.

Peng Y.F., Zhao X., Wu D.H. *et al*. (2018), Spatio-temporal variability in extreme precipitation in China from observations and projections, *Water*, **10**: 1089.

Prein A.F., Rasmussen R.M., Ikeda K. *et al.* (2017), The future intensification of hourly precipitation extremes, *Nature Climate Change*, **7**(1): 48–52.

Seneviratne S., Nicholls N., Easterling D. *et al.* (2012), Changes in climate extremes and their impacts on the natural physical environment: An overview of the IPCC SREX, Report.

Sheffield J., Goteti J. and Wood E.F. (2006), Development of a 50-year high-resolution global dataset of meteorological forcings for land surface modeling, *Journal of Climate*, **19**: 3088.

Sillmann J., Kharin V.V., Zhang X. *et al*. (2013), Climate extremes indices in the CMIP5 multi-model ensemble. Part 1. Model evaluation in the present climate, *Journal of Geophysical Research: Atmospheres*, **118,** 1716–1733.

Suresh S., Geetha R.K., Maheswari M. and Surendran R. (2024), An Automatic Data-Driven Long-term Rainfall Prediction using Humboldt Squid Optimized Convolutional Residual Attentive Gated Circulation Model in India, *Global NEST Journal*, **26**(10), 06421.

Taylor K. (2001), Summarizing multiple aspects of model performance in a single diagram, *Journal of Geophysical Research*, **106**(D7), 7183–7192.

Thrasher B., Wang W., Michaelis A. *et al*. (2022), NASA global daily downscaled projections, CMIP6, *Scientific Data*, **9**: 262.

Wang C.Z., Zhang L.P., Lee S.K. *et al*. (2014), A global perspective on CMIP5 climate model biases, *Nature Climate Change*, **4**: 201–205.

Wang G., Zhang Q., Yu H.Q. *et al*. (2020), Double increase in precipitation extremes across China in a 1.5°C/2.0°C warmer climate, *Science of the Total Environment*, **746**: e140807.

Wang L., Li Y., Li M. *et al*. (2022), Projection of precipitation extremes in China's mainland based on the statistical downscaled data from 27 GCMs in CMIP6, *Atmospheric Research*, **280**, 106462.

Wang X., Jiang D.B. and Lang X.M. (2019), Extreme temperature and precipitation changes associated with four degrees of global warming above pre-industrial levels, *International Journal of Climatology*, **39**, 1822–1838.

Wehner M.F. (2020), Characterization of long period return values of extreme daily temperature and precipitation in the CMIP6 models: Part 2, projections of future change, *Weather and Climate Extremes*, **30**: 100284. https://doi.org/10.1016/j.wace.2020.100284.

Xiang J., Zhang L. and Deng Y. (2021), Projection and evaluation of extreme temperature and precipitation in major regions of China by CMIP6 models, *Engineering Journal of Wuhan University*, **54**(1): 46–57, 81.

Xu Y., Zhou B.T., Wu J. *et al*. (2017), Asian climate change under 1.5−4°C warming targets, *Advances in Climate Change Research*, **8**: 99–107.

Xu H., Chen H. and Wang H. (2022), Future changes in precipitation extremes across China based on CMIP6 models, *International Journal of Climatology*, **42**(1): 635–651.

Yang X.L., Zhou B.T., Xu Y. *et al*. (2021), CMIP6 evaluation and projection of temperature and precipitation over China, *Advances in Atmospheric Sciences*, **38**, 817–830. https://doi.org/10.1007/s00376-021-0351-4.

You Q.L., Sanchez-Lorenzo A., Wild M. *et al.* (2013), Decadal variation of surface solar radiation in the Tibetan Plateau from observations, reanalysis, and model simulations, *Climate Dynamics*, **40**(7–8): 2073–2086.

Yuan Z., Yang Z.Y., Yan D.H. *et al.* (2017), Historical changes and future projection of extreme precipitation in China, *Theoretical and Applied Climatology*, **127**(1–2):393–407. doi:10.1007/s00704-015-1643-3.

Zeng S., Liu Z. and Kaufmann G. (2019), Sensitivity of the global carbonate weathering carbon sink flux to climate and land-use changes, *Nature Communications*, **10,** 5749.

Zhang Y., You Q., Mao G. *et al*. (2019), Short-term concurrent drought and heatwave frequency with 1.5 and 2.0°C global warming in humid subtropical basins: a case study in the Gan River Basin, China, *Climate Dynamics*, **52,** 4621–4641.

Zhang Y.Q., You Q.L., Chen C.C. *et al.* (2024), Characteristics of flash droughts and their association with compound meteorological extremes in China: Observations and model simulations, *Science of the Total Environment*, **916,** 170133. https://doi.org/10.1016/j.scitotenv.2024.170133.

Zhou B.T., Wen Q.Z.H., Xu Y. *et al*. (2014), Projected changes in temperature and precipitation extremes in China by the CMIP5 multi-model ensembles, *Journal of Climate*, **27**: 6591–6611.

Zhou T.J., Zhang W.X., Zhang L.X. *et al.* (2020), The dynamic and thermodynamic processes dominating the reduction of global land monsoon precipitation driven by anthropogenic aerosols emission, *Science China Earth Sciences*, **63**(7): 919–933.

Zhu H.H., Jiang Z.H., Li, J. *et al*. (2020), Does CMIP6 inspire more confidence in simulating climate extremes over China? *Advances in Atmospheric Sciences*, **37**:111–1132. https://doi.org/10.1007/s00376-020-9289-1.

Zhu H., Jiang Z. and Li L. (2021), Projection of climate extremes in China, an incremental exercise from CMIP5 to CMIP6, *Science Bulletin*, **66**(24): 2528–2537.